J. Meas. Sci. Instrum., 2026, 17(1): 49-60. http://jmsi.publish.founderss.cn/
DOI: 10.62756/jmsi.1674-8042.2026004 jmsi@nuc.edu.cn

Pin-retraction detection for aerospace electrical connectors based on binocular stereo vision

ZHANG Xiaolin[1*], LIU Junjie[1], SONG Jianling[2], WANG Meibao[3]

1. School of Instrumentation Science and Engineering, Harbin Institute of Technology, Harbin 150001, China;
2. Capital Aerospace Machinery Co., Ltd, Beijing 100076, China;
3. School of Mechanical Engineering, Zhejiang Sci-Tech University, Hangzhou 310018, China

***Corresponding author:** ZHANG Xiaolin (zhangxiaolin@hit.edu.cn)

Received: August 7, 2025 **Revised:** December 14, 2025 **Accepted:** December 29, 2025

Abstract: Electrical connectors are core functional components in aerospace electrical systems. Pin retraction may lead to signal transmission interruption and even system failure, directly affecting the reliability of electrical equipment and causing incalculable consequences. We propose a high-precision pin-retraction detection method that integrates binocular stereo vision with a multi-constrained optimization matching algorithm, aiming to achieve universal recognition of pins across different connector models and robust detection of pin retraction in complex scenarios. In this study, the Delaunay triangulation algorithm is employed to eliminate the misidentified pins from the template matching algorithm. Furthermore, the pin recognition rate is enhanced to nearly 99.75%, and the accuracy of pin center positioning is significantly improved by integrating a contour fitting and positioning algorithm for pin points. Subsequently, the binocular matching of pins is achieved by combining probabilistic epipolar constraints with geometric constraints, thereby completing the three-dimensional reconstruction of pin points. The Euclidean distance from the three-dimensional pin points to the reference plane is calculated as the pin retraction amount, enabling the quantitative measurement of pin retraction amount. Through the design of multiple experiments for measuring the pin retraction of different-type electrical connectors and the analysis of the results using the Kullback-Leibler (K-L) divergence, it is demonstrated that the system's measurement accuracy is superior to 0.05 mm, with an repeatability error of less than 0.035 mm. The effectiveness of the proposed pin-retraction detection method is thus verified, and the detection efficiency over manual operations is greatly enhanced to meet the actual industrial inspection requirements.

Key words: binocular stereo vision; pin-retraction detection; image processing; electrical connector; machine vision; 3D measurement

0 Introduction

Electrical connectors serve as the fundamental interconnect elements within aerospace assembly systems, spanning multi-level connector requirements and thus constituting an indispensable class of base components[1-3]. Owing to the stringent reliability demands imposed by the complex aerospace environment, even minute failures can precipitate severe consequences. Extensive field data and controlled experiments have established that pin retraction is among the dominant failure modes of electrical connectors[4]. Because connector pins are numerous, miniature, and densely arranged, current pre-installation quality inspection still relies predominantly on manual operators to identify defects such as retraction, offset, or absence[5-7].

Existing strategies for detecting pin retraction include handheld retention-force testing[8]; semi-automated displacement-sensor gauging[9-10]; monocular-vision inspection targeting the entire pin array[11]; 3D point-cloud metrology that incorporates active sensing[12-13]; and binocular stereo-vision based three-dimensional measurement[14]. Hu et al.[15] proposed a semi-automatic displacement-sensor measurement method that requires point-by-point contact; this approach has low efficiency and may cause cumulative damage to the pins during inspection. Zhao et al.[16] captured a large number of high-resolution images of connector pins, including normal pins and defective pins with offset or retraction, and trained different models to learn features from the dataset for retraction detection. Wu et al.[17] proposed an improved YOLOv3-based pin identification algorithm, adding a small-object detection scale to enhance the localization accuracy of tiny pins and employing an

improved Zernike-moment sub-pixel algorithm for edge detection, enabling defect recognition for pins against complex backgrounds; however, these methods require extensive datasets and training, making them unsuitable for industrial measurement. Zhang et al.[18] proposed a laser-triangulation-based coplanarity inspection method for connector pins, combining a camera and a laser to obtain point-cloud data and using RANSAC for plane segmentation and fitting, followed by filtering and clustering to detect coplanarity. Yue et al.[19] employed vision combined with structured light to study a 3D connector defect detection method, scanning pin height via line laser to assess coplanarity. Stroppa L et al.[20] adopted sparse stereo reconstruction, extracting features from two images using a pattern-matching algorithm with pyramidal decomposition and sub-pixel refinement to compute the 3D coordinates of each feature point.

Monocular systems inherently lack depth information, whereas active techniques suffer from algorithmic complexity and intensive computational loads. Binocular stereo vision, by contrast, eliminates dependence on active illumination, offers superior environmental robustness, and provides stable depth resolution; consequently, it has attracted increasing attention from both academia and industry[21]. Existing stereo-vision approaches, however, remain limited by modest accuracy and low inspection efficiency.

Motivated by these observations, we propose a binocular stereo-vision based pin-retraction detection framework for aerospace electrical connectors. We first introduce a template-matching strategy to recognize pins. Shape-based templates combined with Delaunay triangulation eliminate false matches, after which contour centroids of the template regions provide coarse localisation. Subsequent pin-tip contour fitting achieves precise pin localization with a 100% correct-match rate. Second, to solve the binocular correspondence problem for the identified pin features, we exploit the regular pin layout to construct a hierarchical feature model centered on each matched pin. Probabilistic epipolar constraints fused with geometric criteria enable robust left-right feature matching and accurate 3D reconstruction of each pin apex. Finally, to quantify pin retraction quantitatively, circular apertures on the connector housing are detected and employed to fit a reference plane, thereby achieving sequential registration of the pins under test. The Euclidean distance from each reconstructed pin tip to this reference plane is computed, yielding the measured retraction magnitude.

1 Materials and methods

1.1 Elimination of mismatched pins via Delaunay triangulation

The pin identification algorithm is based on template matching, which extracts features from the template and matches them with the search image to locate the template within the image. Given the distinct grayscale characteristics of the pin target regions, a grayscale-based template matching approach is adopted to ensure both accuracy and speed. To mitigate illumination interference, the zero-mean normalized cross-correlation method is employed. Its principle is to compute the cross-correlation between the template and the search image, yielding a correlation coefficient ranging from 0 to 1; a value closer to 1 indicates higher similarity, whereas values near 0 indicate dissimilarity. The normalized correlation coefficient is given as

$$R=\frac{1}{n}\sum_{x,y}\frac{1}{\sigma_f\sigma_t}(f(x,y)-\mu_f)(t(x,y)-\mu_t), \quad (1)$$

where R is the matching correlation coefficient, $f(x, y)$ is the gray value of the search image at that point, $t(x, y)$ is the gray value of the template image at that point, n is the number of pixels in the template image, and σ_f and σ_t are the standard deviations of the image gray values.

Since the pin image contains multiple pin points and template matching involves multi-object identification, the entire image is scanned region by region via a sliding window, extracting the coordinates of centers whose correlation coefficients exceed the preset threshold. The ideal outcome of template matching is that all pins are correctly identified without any false positives. However, in practice, due to illumination and shooting-angle variations, the bright spots of individual pins are not entirely identical, and certain external reflective points caused by lighting may be mistakenly identified as pins. Additionally, printed circuit traces inside the electrical connector can lead to false and omissions, as shown in Fig.1.

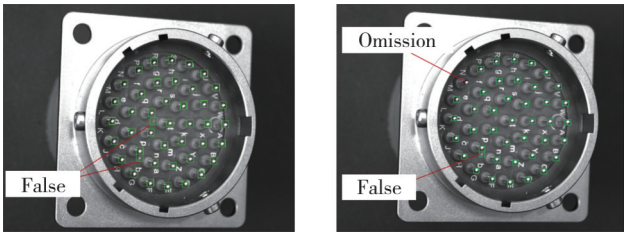

Fig. 1 Cases of false and omission pin detections

To accurately eliminate falsely identified pin points, a structured approach can be introduced based on the spatial geometric characteristics of the pin points, performing

triangulation on the recognized pins. Since the pin point set exhibits geometric consistency in spatial distribution, a super-triangle enclosing all feature points is constructed according to this feature, and the feature points are inserted into the mesh sequentially. Each time a new point is inserted, the triangles related to the point are searched, and the circumcircle of each triangle is calculated. All triangles whose circumcircles contain the new point are recorded, the common edges of these triangles are deleted, new edges are recalculated, and a new triangular mesh is generated. Optimization is performed based on the maximum-minimum angle criterion to obtain the optimized triangular mesh. For each triangle, its three interior angles are calculated. The angle between two vectors is calculated using the vector dot product formula. Given the vertices A, B, C of a triangle, and the angle between the two vectors is calculated as

$$\cos\theta = \frac{\vec{AB} \cdot \vec{AC}}{\left|\vec{AB}\right| \cdot \left|\vec{AC}\right|}. \tag{2}$$

Then, we check whether each interior angle exceeds the threshold: if any triangle contains an out-of-range angle, the vertex actually responsible for the violation is marked as a noise point. The minimum angle threshold was set to 15°, and the maximum angle threshold was set to 100°. These parameters were determined through experimental debugging and systematic analysis of standard pin locations across a wide range of electrical connector types, achieving a false positive rate below 0.1%. All marked points are collected and removed from the original set, yielding a filtered point set with all pins correctly matched. The results before and after outlier removal are shown in Fig.2.

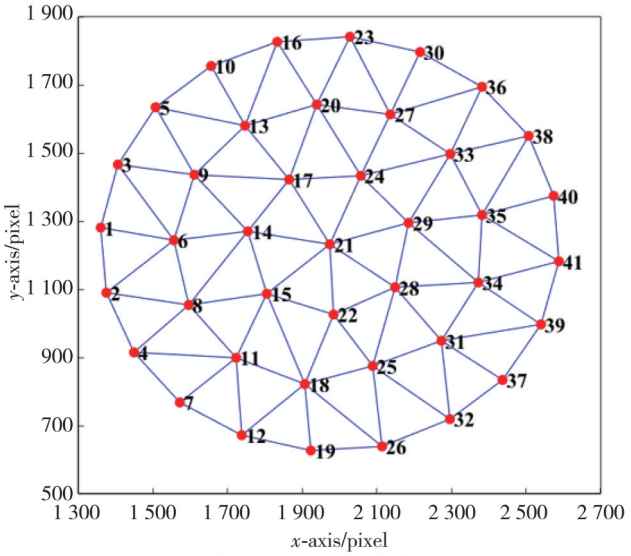

(a) Containing mismatched points

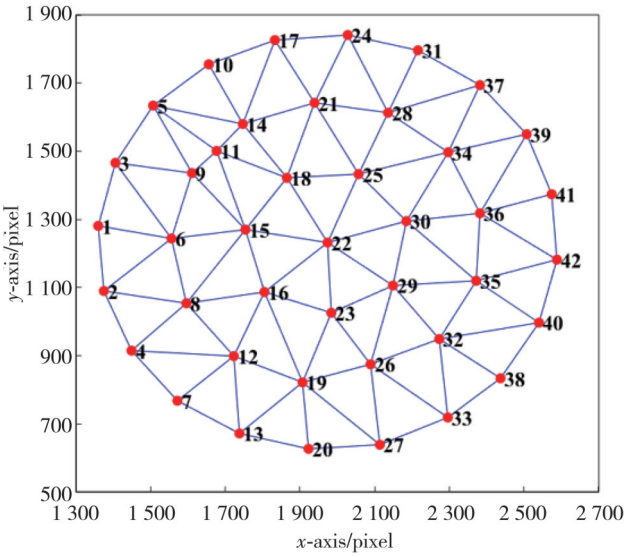

(b) After removing mismatched points

Fig. 2 Triangular mesh schematic before and after removing mismatched points

It should be noted that the Delaunay triangulation algorithm relies on local geometric consistency rather than global arrangement patterns. The method was tested on connectors with typical layouts including rectangular, concentric circular, and array arrangements, and the results demonstrated no significant differences in false rejection rate or missed rejection rate, confirming the robustness of the approach against layout variations.

1.2 Pin-point contour fitting and localization algorithm

Pins exhibit prominent bright-spot characteristics in the image, accompanied by clearly defined edge contours. The centroid of the bright-spot contour is used to determine the tip position of each pin. Canny edge detection is first employed to extract the pin contours; because the pins are small, the resulting edges are highly jagged. Gaussian smoothing is employed to smooth these edges, and the contour centroid is then computed as the pin-tip coordinate, given by

$$x_c = \frac{1}{n}\sum_{i=1}^{n} x_i, \tag{3}$$

$$y_c = \frac{1}{n}\sum_{i=1}^{n} y_i, \tag{4}$$

where n is the total number of pixels within the contour, and x_i and y_i are the coordinates of the ith pixel inside the contour.

Meanwhile, inside the electrical connector, printed lines are used to indicate the arrangement order and index of the pins, and the recognized pin regions contain parts of these printed lines, as shown in Fig.3.

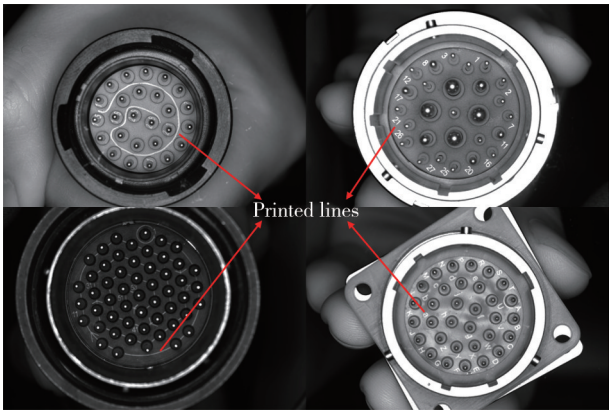

Fig. 3 Pin region containing partial printed lines

The gray-level characteristics of the printed lines are similar to those of the pin bright spots, which affects centroid computation, as illustrated in Fig. 4(a). To eliminate the influence of these printed lines, only the bright-spot portion is retained when processing the pin regions for tip-centroid calculation. The specific steps are as follows: first, edge detection is performed on each matched pin region. If the edges are discontinuous, morphological operations are applied to connect the broken edges, followed by dilation to prevent accidental exclusion of the pin region. Next, a mask is created based on the resulting edge information, filling the interior of the contour with white pixels. Finally, the mask is bitwise-AND with the pin image region to yield the masked image, retaining only the pin region, and the contour center of this region is extracted. Fig.4(b) shows the pin image after masking, and Fig.4(c) presents the extracted pin center obtained after background suppression.

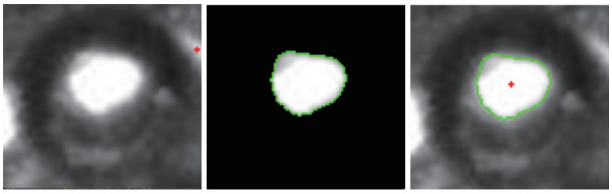

Fig. 4 Pin centroid extraction. (a) Influence of printed wiring on centroid, (b) Mask generation to retain pin region, and (c) Pin centroid without printed-wiring interference

Due to the tilt angle between the camera and the electrical connector during imaging, the reflection positions at the centers of different pins in the captured image of the electrical connector vary. As a result, the centroid coordinates of the pins are not located at the center of the pins but on the side of a quadratic surface centered at the pin tip. Therefore, using only the method of calculating the centroid of the bright spot contour can only provide an approximate position of the pin, not the exact center of the pin.

Based on this, according to the pin-hole imaging model of the quadratic surface, as shown in Fig. 5, the contour of the pin tip is modeled. The center position is calculated based on the modeled surface, and this position is used as the coordinate of the pin center.

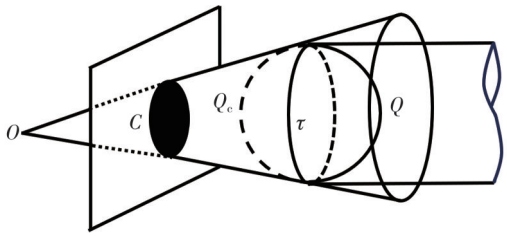

Fig. 5 Pin-hole imaging model of quadratic surface

As shown in Fig. 5, the quadratic surface geometric model of the pin tip can be expressed as a parameterized surface $\boldsymbol{Q}$. The visible contour $\boldsymbol{\tau}$ of this quadratic surface projects onto the image plane as a conic $\boldsymbol{C}$ under projective geometry constraints. According to the contour generation principle, when the camera optical center $\boldsymbol{O}$ and the quadratic surface $\boldsymbol{Q}$ of the pin tip form a visual cone, the intersection of the image plane $\boldsymbol{\Pi}$ and the visual cone yields the contour curve, which can be modeled as

$$\boldsymbol{C}=\boldsymbol{\Pi}\cap\left\{\boldsymbol{X}|\boldsymbol{X}^{\mathrm{T}}\boldsymbol{Q}\boldsymbol{X}=0\wedge\boldsymbol{O}^{\mathrm{T}}\boldsymbol{Q}\boldsymbol{X}=0\right\}. \tag{5}$$

The projection in the image is used to fit the contour τ of the pin tip. Through back projection, contour information is recovered from the projection to fit the pin-tip contour and provide the actual pin position. The specific steps are as follows:

Step 1 Based on blob analysis, connected regions in the region of interest (ROI) are labeled, and the center and area of each blob are extracted. The distance between the largest connected region and each of the others is computed. If the distance exceeds a threshold, the smaller region is judged to be a printed line and filled with black pixels.

Step 2 Using the largest connected region as a seed, region growing is performed toward the remaining small connected regions, and growth stops when no more regions satisfy the expansion criterion.

Step 3 The area and centroid features of the updated region are recalculated, and only the single largest connected region is retained and filled with white pixels inward.

Step 4 An inscribed circle is generated within the updated connected region to create a mask, which is AND with the original ROI to obtain the pin target region.

The above operations are performed on every ROI to yield the pin target region. The brief flowchart is shown in Fig.6, where *thre*1 is the threshold which is related to the size of the electrical connector pin, *thre*2 is the threshold of

the difference between the areas of the maximum and minimum connected regions, whose size is related to the size of the electrical connector pin, and N is the number of pins, which is a parameter known before testing.

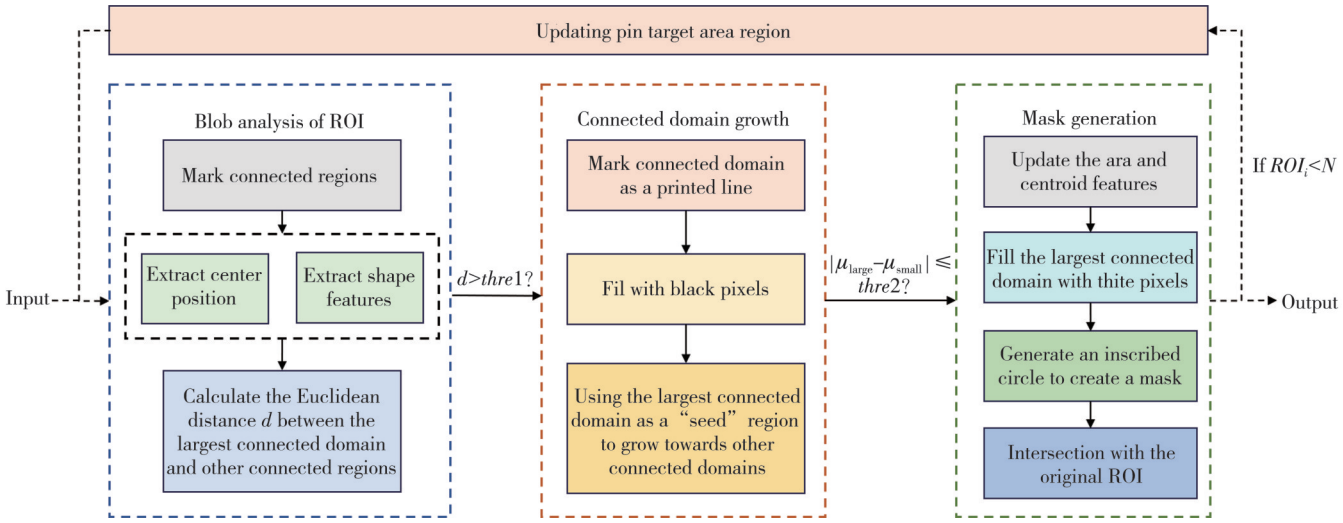

Fig. 6 Pin target region extraction flowchart

The target region extraction result for a single-pin ROI within the electrical connector is shown in Fig.7.

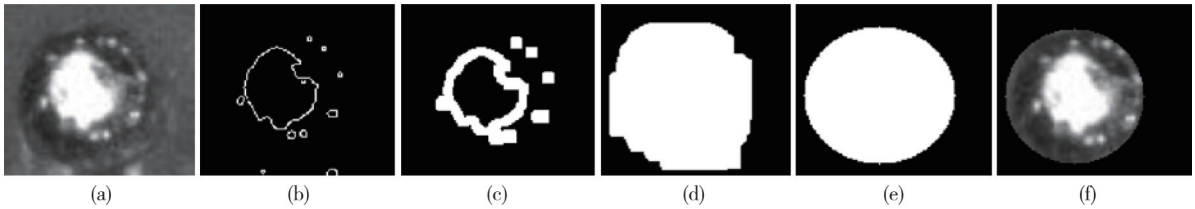

Fig. 7 Pin target region extraction. (a) Original image, (b) Edge extraction, (c) Printed-wiring removal, (d) Region expansion, (e) Inscribed-circle mask, and (f) Pin target

Using the obtained pin target region as the search domain, the algorithm traverses possible circle centers (x_i, y_i) in step increments under a radius constraint:

$$r_k \in \left[\max\left(R_{\min}, \frac{Y_{\text{rect}}}{2}\right), \min\left(R_{\max}, \frac{X_{\text{rect}}}{2}\right) \right]. \tag{6}$$

It is crucial to ensure every candidate circle $C(i,k)$ lies within the search domain and satisfies physical dimensions. For each candidate circle $C(i, k)$, the Bresenham algorithm generates the pixel coordinates $(x_{i,k}, y_{i,k})$ along the circumference. The average brightness $E(P_c)$, the standard deviation $\Delta_{i,k}$, and the skewness $S_{i,k}$ of these circumference pixels are then computed, and a weighting function is designed as

$$H = E(P_c)\left(1 - \frac{\Delta_{i,k}}{\Delta_{\max}}\right)(1 + S_{i,k}). \tag{7}$$

Using the weighting function, the score of each candidate circle is maximized. Candidate circles filtered by skewness are then integrated into a comprehensive evaluation metric, and the circle with the highest confidence is selected as the pin-tip contour. The top-scoring circle is adopted to fit the pin-tip contour and to determine the actual centroid coordinates of the pin.

1.3 Optimization algorithm for feature matching based on probabilistic epipolar constraint

After obtaining the two-dimensional pin coordinates, same-order registration of the pins is required. The epipolar constraint, based on the geometric relationship of binocular vision, simplifies the correspondence matching between images. The epipolar constraint is expressed by

$$\boldsymbol{m}'^{\mathrm{T}} \boldsymbol{F} \boldsymbol{m} = 0, \tag{8}$$

$$\boldsymbol{l}' = \boldsymbol{F}\boldsymbol{m}, \tag{9}$$

where $\boldsymbol{m}$ is a point in the left image, $\boldsymbol{m}'$ is the corresponding point in the right image, $\boldsymbol{l}'$ is the epipolar line passing through $\boldsymbol{m}'$, and $\boldsymbol{F}$ is the fundamental matrix. The fundamental matrix $\boldsymbol{F}$ can be obtained from the intrinsic and extrinsic parameters acquired through calibration as

$$\boldsymbol{F} = \boldsymbol{G}_2^{-\mathrm{T}} \boldsymbol{E} \boldsymbol{G}_1^{-1}, \tag{10}$$

$$\boldsymbol{E} = \begin{bmatrix} 0 & -T_z & T_y \\ T_z & 0 & -T_x \\ -T_y & T_x & 0 \end{bmatrix} \boldsymbol{R}, \tag{11}$$

where $\boldsymbol{G}_1$ and $\boldsymbol{G}_2$ denote the intrinsic matrices of the left and right cameras, respectively; and $\boldsymbol{E}$ is the essential matrix,

which is determined solely by the extrinsic parameters.

In practice, calibration errors of the stereo rig may cause row misalignment between the rectified left and right images, resulting in a pixel-wise vertical offset of the corresponding points. In the pin-highlight regions, which are low-textured and highly repetitive, this residual offset increases the risk of mismatches. Traditional epipolar constraint strictly limits the search to a horizontal line. To accommodate the residual offset, a probabilistic epipolar constraint is introduced, relaxing the search band to $y\pm2$ pixels, allowing $v_r\in[v_l-\Delta y_{max}, v_l+\Delta y_{max}]$, $\Delta y_{max}=2$ pixels. This parameter was determined through calibration tests using stereo image pairs with known ground-truth disparities, with experimental results confirming that the matching error remains lowest within the range of 1 to 3 pixels. The matching score is attenuated using a Gaussian weight expressed as

$$w(v_r)=\exp\left(-\frac{(v_r-v_l)^2}{2\sigma^2}\right), \tag{12}$$

where σ controls the decay rate. Different weights are assigned according to the row offset distance. The matching score at each location is multiplied by the Gaussian weight, and the final matching score is computed as

$$S(u_l,u_r,v_r)=S_{initial}(u_l,u_r)\exp\left(-\frac{(v_r-v_l)^2}{2\sigma^2}\right)=S_{initial}(u_l,u_r)w(v_r). \tag{13}$$

Based on the candidate point with the highest matching score, the edge at position (x, y) is examined, and the Sobel operator is used to compute the gradient (G_x, G_y). Assuming the gradient attains an extremum at the sub-pixel location $(x+\delta x, y+\delta y)$, a quadratic interpolation model is adopted as

$$\begin{aligned}\delta_x&=-\frac{G_x}{2G_{xx}},\\ \delta_y&=-\frac{G_y}{2G_{yy}},\end{aligned} \tag{14}$$

where G_{xx} and G_{yy} are the second-order gradients, and the sub-pixel coordinates are then obtained as

$$(x_s,y_s)=(x+\delta_x,y+\delta_y). \tag{15}$$

Based on the obtained sub-pixel coordinates, the epipolar search range is refined. Using the probabilistic epipolar constraint model, the geometric correspondence of pin feature points is effectively confined within a unipolar epipolar domain. By introducing an additional consistency constraint in the orthogonal dimension, a bilinear constraint equation is constructed, enabling a closed-form solution for the pixel coordinates of conjugate image points. The pin points derived from clustering are assigned to different hierarchical levels and reordered according to point-set density, thereby enhancing inter-level matching robustness.

Establishing an initial correspondence between the angle-sorted points of the left and right images not only reduces global search complexity but also preserves rotational consistency of the pin points, preventing blind matching. To further guarantee matching accuracy, a hierarchical RANSAC algorithm is incorporated for geometric-consistency verification and outlier removal. Its core idea is to partition all pin correspondences into multiple subsets according to a priori geometric rules, and at each level independently perform model fitting and outlier rejection. The main procedure takes the pin point set $P=\{C_1,C_2,\cdots,C_k\}$ as input, where C_k denotes the pin point subset at level k, and sets a dynamic residual threshold as

$$\theta_k=\alpha r_k, \tag{16}$$

where r_k is the layer radius, and α is the empirical coefficient (typically 0.01).

For layer k, the disparity model is assumed to be linear,

$$x_r=a_kx_l+b_k+\sigma, \tag{17}$$

where x_l and x_r are the horizontal coordinates of the matched points in the left and right images, respectively, and $\sigma\sim N(0,\sigma^2)$ is the noise term. A minimal dataset is randomly sampled from the current layer C_k to generate a candidate model, and the model parameters a_k and b_k are solved using the least-squares method

$$\min_{a_k,b_k}\sum_{(x_l,x_r)\in S_{min\,s}}\left\|x_r-(a_kx_l+b_k)\right\|^2, \tag{18}$$

where $S_{min\,s}$ is the minimal sample set.

Thus, we count the points that satisfy the residual condition by

$$I_k=\left\{(x_l,x_r)\in E_k\middle|\,|x_r-(a_kx_l+b_k)|<\sigma_{th,k}\right\}. \tag{19}$$

If a matched point satisfies the residual condition, it is classified as an inlier; otherwise, it is judged an outlier. The above steps are repeated iteratively to obtain the final estimate, and the matching results are presented in Section 2.1.

1.4 Three-dimensional reconstruction of sparse points and pin-retraction detection

After the recognition and matching of the pin points in the electrical connector, we have already obtained the position coordinates of the pins and the correspondence between the same pins in the left and right images. To further obtain the depth relationship of the pins, we first need to set the 3D coordinates of the centroid P of the pin tip as (X, Y, Z), and the pixel coordinates of this point in the left and right

cameras are $p_l(u_l, v_l)$ and $p_r(u_r, v_r)$, respectively. The depths s_l and s_r of point P in the Z direction of the left and right camera coordinate systems are then calculated as

$$s_l\begin{bmatrix}u_l\\v_l\\1\end{bmatrix}=\begin{bmatrix}m_{11}^l & m_{12}^l & m_{13}^l & m_{14}^l\\m_{21}^l & m_{22}^l & m_{23}^l & m_{24}^l\\m_{31}^l & m_{32}^l & m_{33}^l & m_{34}^l\\m_{41}^l & m_{42}^l & m_{43}^l & m_{44}^l\end{bmatrix}\begin{bmatrix}X\\Y\\Z\\1\end{bmatrix}=\boldsymbol{M}_l\begin{bmatrix}X\\Y\\Z\\1\end{bmatrix},\quad(20)$$

$$s_r\begin{bmatrix}u_r\\v_r\\1\end{bmatrix}=\begin{bmatrix}m_{11}^r & m_{12}^r & m_{13}^r & m_{14}^r\\m_{21}^r & m_{22}^r & m_{23}^r & m_{24}^r\\m_{31}^r & m_{32}^r & m_{33}^r & m_{34}^r\\m_{41}^r & m_{42}^r & m_{43}^r & m_{44}^r\end{bmatrix}\begin{bmatrix}X\\Y\\Z\\1\end{bmatrix}=\boldsymbol{M}_r\begin{bmatrix}X\\Y\\Z\\1\end{bmatrix},\quad(21)$$

where $\boldsymbol{M}_l$ and $\boldsymbol{M}_r$ are the projection matrices of the left and right cameras, respectively; $(u_l, v_l, 1)$ and $(u_r, v_r, 1)$ are the homogeneous coordinates of the pin-tip centroid P in the image coordinate system; and $(X, Y, Z, 1)$ is the homogeneous coordinate of point P in the world coordinate system. Simplifying Eqs. (20) and (21) yields

$$\begin{cases}(u_lm_{31}^l-m_{11}^l)X+(u_lm_{32}^l-m_{12}^l)Y+\\\quad(u_lm_{33}^l-m_{13}^l)Z=m_{14}^l-u_lm_{34}^l,\\(u_lm_{31}^l-m_{21}^l)X+(u_lm_{32}^l-m_{22}^l)Y+\\\quad(u_lm_{33}^l-m_{23}^l)Z=m_{24}^l-u_lm_{34}^l,\\(u_rm_{31}^r-m_{11}^r)X+(u_rm_{32}^r-m_{12}^r)Y+\\\quad(u_rm_{33}^r-m_{13}^r)Z=m_{14}^r-u_rm_{34}^r,\\(u_rm_{31}^r-m_{21}^r)X+(u_rm_{32}^r-m_{22}^r)Y+\\\quad(u_rm_{33}^r-m_{23}^r)Z=m_{24}^r-u_rm_{34}^r.\end{cases}\quad(22)$$

The linear system of Eq. (22) can be solved using the least-squares method to obtain the 3D coordinates of point P, thereby yielding the 3D coordinates of the pin point.

Obtaining the 3D coordinates of the pin signifies the completion of the measurement of the pin's depth information. Subsequently, it is necessary to determine the extent of deviation in depth for a pin to be classified as retracted. Based on the obtained 3D coordinates of the pin points $P(x_i, y_i, z_i)$, the directed distance from each pin point to the fitted reference plane is calculated as

$$h_i=\frac{Ax_i+By_i+Cz_i+D}{\sqrt{A^2+B^2+C^2}}.\quad(23)$$

The histogram method is used for binning statistics, and the number of intervals K is determined using Sturges' rule as

$$K=\lceil\log_2^n\rceil+1.\quad(24)$$

The probability $P(i)$ of each interval and the number of samples $K(i)$ falling into each interval i are calculated by

$$P(i)=\frac{K(i)}{n}.\quad(25)$$

Assuming that the fluctuation of the pin follows a zero-mean Gaussian distribution, the Gaussian distribution is calculated for each histogram interval i as

$$Q(i)=F\left(\frac{b_i-0}{0.1}\right)-F\left(\frac{a_i-0}{0.1}\right),\quad(26)$$

where $F(\cdot)$ is the cumulative distribution function.

Kullback-Leibler (K-L) divergence is used to quantify the difference between the actual distribution P and the theoretical distribution Q as

$$D_{KL}(P\|Q)=\sum_{i=1}^{K}P(i)\ln\left(\frac{P(i)}{Q(i)+\varepsilon}\right),\quad(27)$$

where ε is a small perturbation added to the theoretical distribution probability to avoid an analytical solution when $Q(i)=0$, and ε is taken as 10^{-6}.

2 Results and discussion

To meet the requirements of the electrical connector quality inspection system, which aims to reduce the constraints on the degrees of freedom of the electrical connectors while achieving high-precision measurement, the inspection equipment mainly consists of an LED strip light source, an industrial camera and lens, and a stereo camera experimental stand. The binocular vision system was constructed using two industrial cameras, each with a resolution of 3 088×2 064 pixels and a pixel size of 2.4 μm, equipped with lenses having a focal length of 150 mm. The baseline distance between the two cameras was set to 74 mm. The inspection process is generally as follows: According to the algorithm proposed in this paper, first, the intrinsic and extrinsic parameters of the camera are obtained through camera calibration, and stereo rectification is performed to align the left and right images on the same horizontal plane. Subsequently, the pins of the electrical connector image are identified, and the center points of the pins are located. Next, the optimized matching algorithm is used to match the pin points and reconstruct their three-dimensional coordinates. Finally, the pin retraction is detected.

2.1 Test of pin center identification and matching

To verify the effectiveness of the pin center identification and localization algorithm, six different types of electrical connectors: JY27497E55, JY27472T20F41, Y11X1626, 3027, 26JH53PN, and J14A-74TJ, were each subjected to pin tip center identification tests, as shown in Fig.8. We tested over 300 pin images of more than 10 types of electrical connectors. The algorithm proposed in this paper was able to effectively identify the pins of electrical connectors in all cases. It can be concluded that the correct

recognition rate is close to 100%, and the precise coordinates of the pin centers can be extracted.

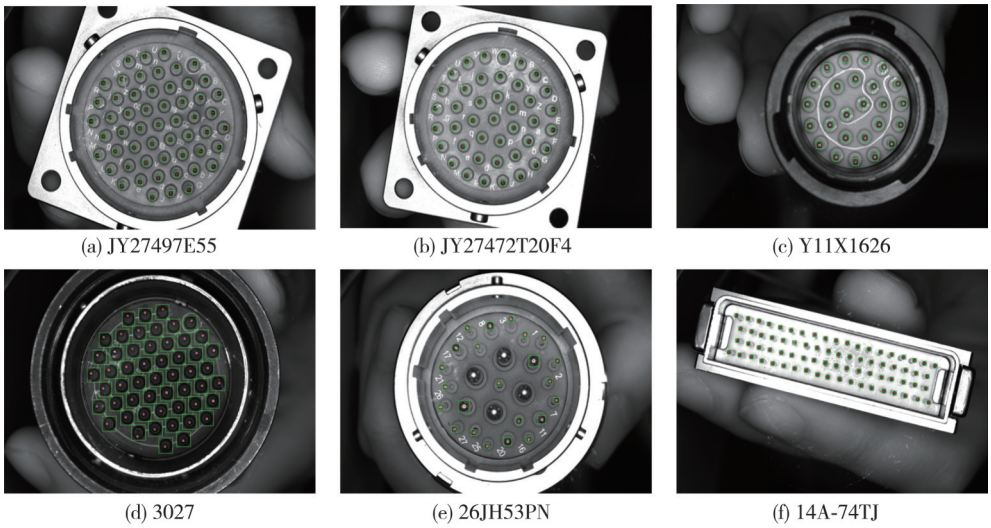

Fig. 8 Results of pin center identification, where green box indicates pin area and red dot indicates pin center

To verify the optimization algorithm for feature matching based on probabilistic epipolar constraint, the electrical connector JY27472T32 was selected for hierarchical matching. Since the geometric feature of the pins in the JY27472T32 electrical connector is a concentric circular arrangement (which is the case for most electrical connectors), the pins in the left and right images of the JY27472T32 were matched hierarchically from the largest to the smallest radius. The successful matching is demonstrated by connecting the same pin with a single line. The pin matching results of JY27472T32 are shown in Fig.9.

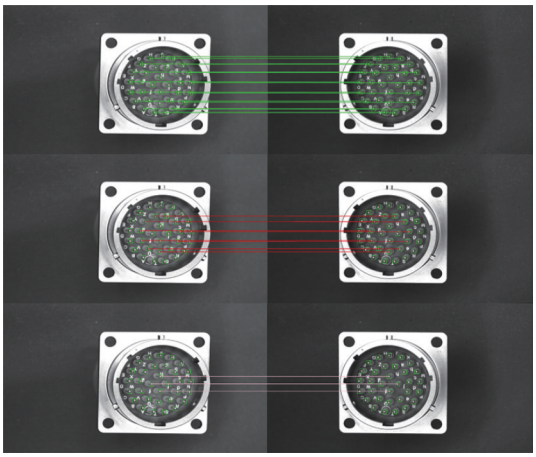

Fig. 9 Pin matching results of connector JY27472T32 (green lines: outer pins; red lines: middle pins; pink lines: inner pins)

2.2 Pin-retraction determination

In order to verify the accuracy and repeatability of the pin-retraction detection algorithm, one pin was manually selected and its depth along the Z-axis was altered for four different types of electrical connectors, namely JY27472T20F41, JY27472T32, JY27497E55, and 15TJ. Subsequently, images of the electrical connectors were captured, and the depth information of each pin center of the electrical connectors was extracted using the algorithm proposed in this paper. The extracted depth information was then compared with the results measured by a coordinate measuring machine (with an accuracy of 0.001 mm). Finally, the detection results were analyzed.

To ensure the generality of the experimental results, each type of electrical connector was tested at least 10 times in different orientations to obtain stable data for calculating the average value. The algorithm used relative measurement, with the relative distance from the pin point to the fitted reference plane serving as the basis for judging the height of the pin and detecting the presence of pin retraction. Fig. 10 shows the statistical results of five measurements of pins for different types of electrical connectors. In this figure, the values on the x-axis represent the pin numbers, while the values on the y-axis represent the distances between the pin centers and the reference plane of the detection system. Furthermore, to address potential concerns regarding the reference plane fitting, which is a critical step in deriving the retraction magnitude, a robustness analysis was conducted.

The circular apertures on the connector housing, which are used to fit this plane, are significantly larger than the pins. Our analysis confirms that a circular edge positioning error of 0.1 pixel introduces a deviation in the fitted reference plane of less than 0.005 mm. This error is negligible compared to the system's verified measurement accuracy of 0.05 mm, thereby ensuring the reliability of the retraction measurement.

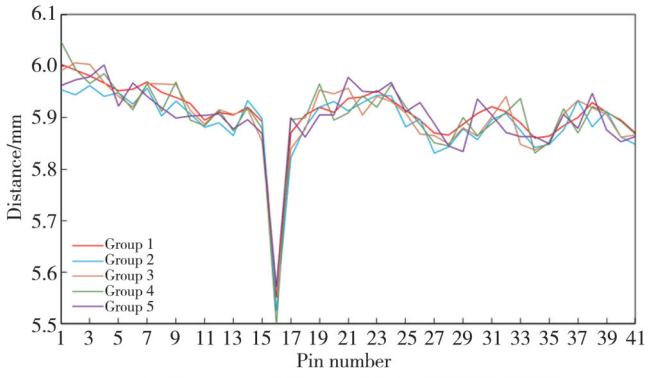

(a) Five groups of distance data for JY27472T20F41

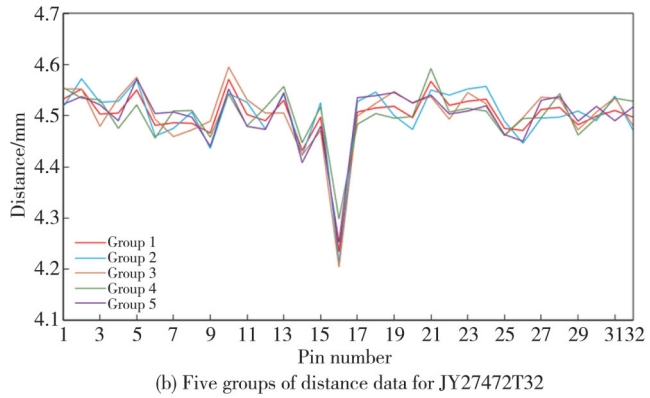

(b) Five groups of distance data for JY27472T32

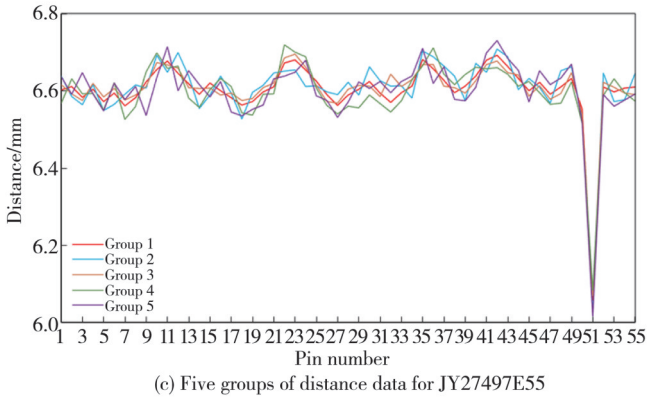

(c) Five groups of distance data for JY27497E55

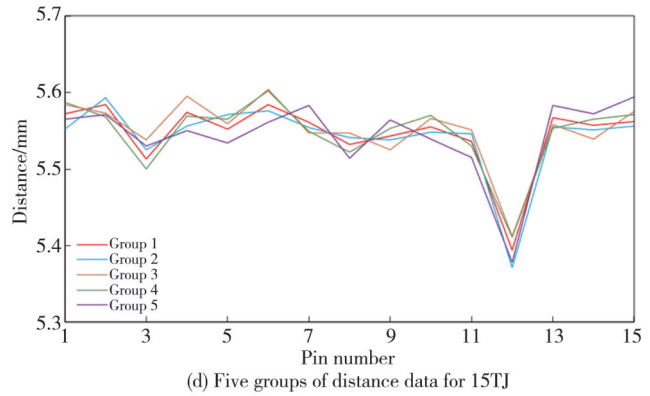

(d) Five groups of distance data for 15TJ

Fig. 10 Statistical results of five measurements for different connector models

From the detection results of different types of pins, it can be seen that for the same pin point, the maximum standard deviation in multiple measurements is 0.04 mm, indicating good measurement stability; under the condition of equal-precision measurement, the repeatability error is 3.7%, showing good measurement repeatability. Here, the pin-retraction measurement data of the JY27513E55 electrical connector is taken as an example for analysis. For comparison, a coordinate measuring machine (CMM) was employed to obtain the standard height of each pin relative to the same fitted plane. Table 1 compares the pin retraction results, where the measured value represents the mean of 10 repeated measurements obtained by our method, and the standard value is the corresponding mean derived from CMM measurements under the same condition. The range shown in the table indicates the variation (maximum minus minimum) of the 10 measurements from our method. Only the results for the first 15 pins and the 51st abnormal pin of the JY27513E55 are listed.

Table 1 Comparison of measured pin-tip height and standard height for JY27513E55 (list only the first 15 pins and the 51st abnormal pin)

Serial No.	Measured value/mm	Standard value/mm	Range/mm	Repeatability error/mm
Pin 1	0.025	0.020	0.049	0.015
Pin 2	0.043	0.046	0.028	0.009
Pin 3	0.076	0.039	0.036	0.017
Pin 4	0.043	0.022	0.040	0.012
Pin 5	0.020	0.029	0.003	0.030
Pin 6	0.033	0.033	−0.025	0.024
Pin 7	0.004	0.025	−0.017	0.024
Pin 8	0.019	0.025	0.007	0.025
Pin 9	0.020	0.004	0.003	0.019
Pin 10	0.027	0.001	0.001	0.035
Pin 11	0.013	0.009	0.038	0.018
Pin 12	0.010	0.057	−0.044	0.031
Pin 13	0.051	0.072	−0.042	0.026
Pin 14	0.077	0.074	−0.035	0.027
Pin 15	0.020	0.037	−0.004	0.022
Pin 51 (abnormal)	**0.448**	**0.457**	**−0.013**	**0.013**

From the data in Table 1, it can be concluded that the average deviation of pin height detection using the pin-retraction detection method proposed in this paper is within 0.05 mm. Additionally, the repeatability error was calculated using statistical methods. Based on 10 measurement results, the maximum repeatability error was 0.035 mm, indicating a high measurement accuracy. The standard retraction of pin 51 was 0.457 mm (pins measured using a coordinate measuring machine), while the pin retraction measured by the method described in this paper was 0.448 mm, with a deviation of only 0.013 mm.

In addition, to quantitatively evaluate the detection efficiency, processing speed tests were conducted on a platform equipped with an NVIDIA GeForce RTX 4060 GPU. The system achieved an average processing speed of 10 frame per second. This represents an orders-of-magnitude improvement in detection efficiency compared

to the sensor-based manual handheld measurement methods currently prevalent in China for pin-retraction detection, effectively overcoming the limitations of low efficiency and operator-dependent results inherent in traditional approaches.

After obtaining the relatively accurate depth information of the pin centers of the electrical connectors using the algorithm proposed in this paper, we need to focus on the judgment of the pin-retraction situation, as mentioned in Section 1.4.

The K-L divergence is used to measure whether there is pin retraction in the electrical connector. The value of the K-L divergence is sensitive to the tail of the theoretical probability distribution. If the actual distribution contains outliers, the value of D_{KL} will increase significantly, indicating the presence of pin retraction. Taking the pin detection data of the JY27497E55 electrical connector as an example, given that the total number of samples is 55, the number of intervals is determined to be 7 according to Sturges' rule. The distribution of distance values is shown in Fig.11, and the result of the K-L divergence is shown in Table 2.

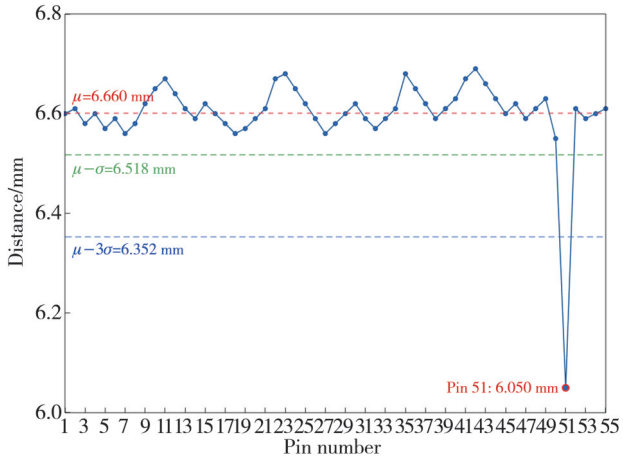

Fig. 11 Distribution of distances from pins of JY27513E55 electrical connector to reference plane

Table 2 Results of K-L divergence

Interval No.	$P(i)$	$Q(i)+\varepsilon$	$P(i)\ln\left(\frac{P(i)}{Q(i)+\varepsilon}\right)$
1	0.018 2	0.000 200 01	0.082 1
2	0	0.016 000 01	0
3	0	0.222 700 01	0
4	0.127 3	0.522 200 01	−0.179 6
5	0.672 7	0.222 700 01	0.746 7
6	0.145 5	0.016 000 01	0.321 3
7	0.036 4	0.000 200 01	0.189 3

The K-L divergence D_{KL} is calculated to be 1.16. The discrimination threshold for D_{KL} is not fixed but is adaptively determined based on the total number of pins (N) via Monte Carlo simulation. For this connector (N=55, belonging to the $N>30$ category), the 95% quantile threshold is established at 0.12. This threshold, along with others for different pin counts, was derived by generating 10 000 sets of normally distributed samples for each category and calculating the 95% quantile of the resulting D_{KL} distribution:

For $N\leqslant 15$ s, the threshold is 0.20.

For $16\leqslant N\leqslant 30$, the threshold is 0.15.

For $N>30$, the threshold is 0.12.

Therefore, it can be concluded that the actual calculated D_{KL} value of 1.16 is much greater than the applicable threshold of 0.12, indicating the presence of pin retraction. According to the 3σ rule, points with an absolute height value exceeding $3\sigma = 0.249$ mm can be marked as retracted pins. As shown in Figs.12 and 13, the height value of pin number 51 meets the 3σ criterion, confirming it as a retracted pin, while the other pins fluctuate within the range of 6.5—6.7 mm.

Using the proposed algorithm, six types of electrical connectors were inspected. For each type, 200 images were captured, and the 3σ criterion was applied to identify pin retraction. Among the 1 200 images, 1 197 accurately detected the serial numbers of the retracted pins, while 3 images experienced missed detections, resulting in a pin recognition rate of 99.75%.

3 Conclusions

This research proposes a pin identification and localization algorithm based on template matching, which can effectively recognize and locate electrical connectors with the same pin shape but different arrangements and sizes. Combined with Delaunay triangulation for eliminating mismatched pins, it achieves a pin identification accuracy of 99.75%, overcoming the limitation of monocular vision being only applicable to exposed pin detection. By integrating probabilistic epipolar constraints with the geometric characteristics of pin arrangement distribution, hierarchical matching of pin feature points is realized, improving matching efficiency and accuracy.

In addition, a method for fitting the reference plane of electrical connector pins is designed. By calculating the relative distance from the 3D reconstructed pin points to the fitted plane, pin retraction detection is achieved, and the measurement results are analyzed using K-L divergence. The experimental results show that the accuracy of the measurement system was better than 0.05 mm, which verifies the effectiveness of the pin-retraction detection.

Acknowledgement

This work was supported by National Natural Science

Foundation of China-Youth Program (No. 62303420), and thank you to all the researchers who participated in this article for their hard work and contribution.

Declaration of conflicting interests

The authors have no conflict of interests related to this publication.

References

[1] ZHANG X L, LIU J J, BAI L Q, et al. Machine vision-based electrical connector pin identification and quality inspection method research. Mechanical Instrumentation and Automation, Journal of Physics: Conference Series, 2025, 3032(1): 012025.

[2] LI Z P. Review of key technologies for electrical connector contacts. Electromechanical Components, 2014, 34(4): 5.

[3] LU J. Research on Pin Inspection Technology for Aerospace Electrical Connectors Based on Machine Vision. Dissertation for the Master Degree. Harbin: Harbin Institute of Technology, 2017: 10-14.

[4] SUN R, HUANG J, GAO C, et al. Failure modes and critical process analysis of separation-release electrical connectors. Electromechanical Components, 2019, 39(1): 20-25.

[5] LIU X Y. Analysis of failure modes of electrical connectors. Electromechanical Components, 2017, 37(1): 53-54.

[6] WANG Y C. Research on detection system of terminal high and low pins based on machine vision. Dissertation for the Master Degree. Harbin: Heilongjiang University, 2018: 3-10.

[7] LI J, REN C, XU J, et al. Skewed pins detection of aviation connectors based on multi-modal cooperative perception// 2024 International Conference on Artificial Intelligence of Things and Systems, October 17-19, 2024, Hangzhou, China. New York: IEEE, 2014: 1-6.

[8] GAO S D, ZHU C F, XUE C. Rapid detection device and method for pin retraction of circular electrical connectors. China Patent, CN107091942 B, 2019-06-07.

[9] SU X, FAN J, YANG Y, et al. Pin-retraction detection method for electrical connectors based on piezoresistive effect. Machine Building & Automation, 2018, 47(5): 242-245.

[10] JI H, HSU H Y, KONG L X, et al. Development of a contact probe incorporating a Bragg grating strain sensor for nano coordinate measuring machines. Measurement Science and Technology, 2009, 20(9): 095304.

[11] HAN Y, YAO Y, YANG X, et al. Research on connector pin retraction and bending detection system based on machine learning. Automation & Instrumentation, 2022, 37: 57–60.

[12] DU Q, LI D, CHEN H, et al. Pin-tip extraction from structured-light 3D point clouds. Chinese Journal of Liquid Crystals and Displays, 2021, 36(9): 1331-1340.

[13] GONG Y, DU S, WANG Z G, et al. Pillow spring height measurement method based on 3D point cloud processing. Journal of Test and Measurement Technology, 2025, 39(1): 63-71.

[14] LIU W C, YANG Y R, WANG W, et al. Orthogonality inspection method for connector pins using binocular vision. Laser & Optoelectronics Progress, 2023, 60(14): 289-297.

[15] HU Y. Design of automatic pin-retraction detection system for electrical connectors. Harbin: Harbin Institute of Technology, 2020: 5-8.

[16] ZHAO Y Y, LI J, ZHANG Q Y, et al. Simultaneous detection of defects in electrical connectors based on improved convolutional neural network. IEEE Transactions on Instrumentation and Measurement, 2022, 71: 3511710.

[17] WU P F. Research on pin detection technology for automotive electronic connectors based on machine vision. Guilin: Guilin University of Electronic Technology, 2020: 6-8.

[18] ZHANG Y, LI X, ZHANG W. Detection of coplanarity of connector pins based on laser triangulation. Transducer and Microsystem Technologies, 2020, 39(9): 154-156.

[19] YUE J, YANG C, LI S, et al. 3D defect detection of connectors based on structured light. Optoelectronics Letters, 2021, 17(2): 107-111.

[20] STROPPA L, CRISTALLI C. Stereo vision system for accurate 3D measurements of connector pins' positions in production lines. Experimental Techniques, 2017, 41(1): 69-78.

[21] YANG C, LU W Z, XIA Y Q. Positioning accuracy analysis of industrial robots based on non-probabilistic time-dependent reliability. IEEE Transactions on Reliability, 2024, 73(1): 608-621.

基于双目立体视觉的航天电连接器缩针检测技术

张晓琳[1*], 刘俊杰[1], 宋建岭[2], 王梅宝[3]

1. 哈尔滨工业大学 仪器科学与工程学院, 黑龙江 哈尔滨 150001;
2. 首都航天机械有限公司, 北京 100076;
3. 浙江理工大学 机械工程学院, 浙江 杭州 310018

摘　要： 电连接器是航天电气系统中的核心功能组件，缩针会导致信号传输中断甚至系统失效，直接影响电气设备可靠性，带来不可估量的后果。本文提出一种融合双目立体视觉与多约束优化匹配算法的高精度缩针检测方法，旨在实现各型号电连接器插针的通用化识别，针对缩针实现高精度检测及复杂场景下的鲁棒性检测。提出了基于模板匹配算法实现插针区域识别，采用Delaunay三角剖分算法剔除误识别插针，结合插针点轮廓拟合定位算法，将插针识别率提升至99.75%，且大大提高插针中心定位精度。其次，通过概率极线约束结合几何约束特性实现插针双目匹配，完成插针点的三维重建，并计算插针三维点至基准平面的欧式距离作为缩针量，实现缩针量的定量测量。通过设计多组不同型号的电连接器缩针测量实验并利用K-L散度分析结果可知，系统检测精度优于0.05 mm，重复误差在0.035 mm以内，验证了所提出的缩针检测方法的有效性，并大大提高了检测效率，满足实际工业检测需求。

关键词： 双目立体视觉；缩针检测；图像处理；电连接器；机器视觉；三维测量

引用格式： ZHANG Xiaolin, LIU Junjie, SONG Jianling, et al. Pin-retraction detection for aerospace electrical connectors based on binocular stereo vision. Journal of Measurement Science and Instrumentation, 2026, 17(1): 49-60. DOI: 10.62756/jmsi.1674-8042.2026004